A phase-field approach to pneumatic fracture

Carola Bilgen[1,*], **Alena Kopaničáková**[2], **Rolf Krause**[2], and **Kerstin Weinberg**[1]

[1] Universität Siegen, Paul-Bonatz-Str. 9-11, 57076 Siegen, Germany
[2] USI- Universitá della Svizzera italiana, Via Giuseppe Buffi 13, 6900 Lugano, Switzerland

Phase-field methods for brittle fracture employ a variational framework and have proven to predict complex fracture patterns in two and three dimensional examples. This contribution focuses on a phase-field approach for a coupled field model of brittle pneumatic fracture. Two different challenges are tackled in this contribution: First, we have to deal with pressure-driven processes within the proposed phase-field ansatz, second, we have to consider the numerical effort of the simulations.

Our phase-field formulation is based on elasticity and a suitable operator split to take only the tensile parts into account. Furthermore, a prescribed pressure is coupled with the phase-field parameter to consider crack propagation induced by pneumatic pressure. To keep the numerical effort as small as possible we apply a specifically developed multigrid method for three-dimensional problems. The accuracy and the robustness of the solution method will be demonstrated with a series of numerical examples.

1 Introduction

The focus is set on phase-field models for brittle fracture in the context of both, finite and linearized strains. Let us consider a solid with domain $\Omega \subset \mathbb{R}^3$ and a boundary $\partial\Omega \subset \mathbb{R}^2$ deforming within a time interval $t \in [0, T] \subset \mathbb{R}^+$. The creation of new surface leads to an energetic contribution to the total potential energy which consists of the configurational and interface energy; others might be added as well. In the phase-field approach an order parameter $\mathfrak{s}(\mathbf{x}, t)$ is introduced which marks the material's state of the body with domain Ω and evolves in space $\mathbf{x}$ and time t. The surface integral is approximated by a weighted integration over the domain Ω, enforced by a crack density function $\gamma(\mathfrak{s})$ which is positive along the crack region and zero otherwise. There is no unique way to choose the crack density function γ. In the following we apply the second-order phase-field approach $\gamma(\mathfrak{s}, \nabla\mathfrak{s}) = \frac{1}{2l_c}\mathfrak{s}^2 + \frac{l_c}{2}|\nabla\mathfrak{s}|^2$ with length-scale parameter l_c which is a measure for the width of the diffuse interface zone and weights the influence of the linear and the gradient term. Within this regularization the total potential energy can be formulated as follows:

$$E = \int_\Omega \Psi \, \mathrm{d}\Omega + \int_{\partial\Omega} \mathcal{G}_c \, \mathrm{d}(\partial\Omega) \approx \int_\Omega (\Psi + \mathcal{G}_c\gamma) \, \mathrm{d}\Omega \tag{1}$$

The strain energy density of the body is denoted by $\Psi(\mathbf{u}, ...)$ and the specific fracture energy by $\mathcal{G}_c$. The fracture energy density $\mathcal{G}_c$ quantifies the material's resistance to cracking and corresponds to Griffith's critical energy release rate for brittle fracture. The evolution equation of the phase-field is defined in a general form $\dot{\mathfrak{s}} = MY$ where the parameter M denotes the kinematic mobility and Y summarizes all driving forces. In the following the driving force of the phase-field Y is given in its variational form $Y = \frac{\partial\Psi}{\partial\mathfrak{s}}$.

2 Governing equations

2.1 Fracture in linear elasticity

In classical linear elasticity the strain energy function is defined as $\Psi(\epsilon) = \frac{1}{2}\epsilon(\mathbf{u}) : \mathbb{C}^\star(\mathfrak{s}) : \epsilon(\mathbf{u})$ where $\epsilon(\mathbf{u}) = \mathrm{sym}(\nabla\mathbf{u})$ is the strain energy tensor, and $\mathbb{C}^\star = g(\mathfrak{s})\mathbb{C}$ is the adapted elasticity tensor with a degradation function $g(\mathfrak{s})$ to express a local damage of the material in the model. The degradation function can be chosen in different ways as long as the conditions $g(0) = 1$, $g(1) = 0$ and $g'(1) = 0$ are fulfilled. We choose the simplest degradation function $g(\mathfrak{s}) = (1-\mathfrak{s})^2$ in the following. In order to take into account that only tensile stresses contribute the crack propagation, the strain energy function is split into a tensile and a compressive part. Only the tensile part is influenced by the phase-field parameter:

$$\Psi^e(\mathbf{u}, \mathfrak{s}) = g(\mathfrak{s})\Psi_n^{e+} + \Psi_n^{e-} \tag{2}$$

with $\Psi_n^{e\pm} = \frac{1}{2}\epsilon^\pm(\mathbf{u}) : \mathbb{C} : \epsilon^\pm(\mathbf{u})$. In Table 1 an overview about the total minimization problem is given.

* Corresponding author: e-mail carola.bilgen@uni-siegen.de

Balance of linear momentum:	Boundary conditions:	Phase-field:	Boundary conditions:
$\mathrm{Div}(\boldsymbol{\sigma}) + \bar{\mathbf{b}} = \rho_0 \ddot{\mathbf{u}}$ on Ω	$\mathbf{u} = \bar{\mathbf{u}}$ on $\partial\Omega$	$\mathfrak{s} - l_c^2 \triangle \mathfrak{s} = 0$ on Ω	$\nabla \mathfrak{s} \cdot n = 0$ on $\partial\Omega$
	$\boldsymbol{\sigma} \cdot n = \bar{q}$ on $\partial\Omega$		$\mathfrak{s} = 0$ on $\partial\Omega$

Table 1: Total minimization problem

2.2 Fracture in finite elasticity

The general concept of Griffith's critical energy release rate and the corresponding potential energy (1) is limited to brittle fracture but does not presume small deformations. The approach is also valid in the finite deformation regime with deformation mapping $\chi(\mathbf{X}, t) : \Omega \times [0, T] \to \mathbb{R}^3$ and the kinematic set which is given in Table 2.

Deformation gradient $\mathbf{F}$	$\mathbf{F} : \Omega \times [0, T] \to \mathbb{R}^{3\times3}$	$\mathbf{F} = \nabla_{\mathbf{X}} \chi = \frac{\partial \chi}{\partial \mathbf{X}}$
Cofactor $\mathbf{H}$	$\mathbf{H} : \Omega \times [0, T] \to \mathbb{R}^{3\times3}$	$\mathbf{H} = \mathrm{cof}(\mathbf{F}) = \frac{1}{2}(\mathbf{F} \times \mathbf{F})$
Volume map J	$J : \Omega \times [0, T] \to \mathbb{R}$	$J = \det(\mathbf{F}) = \frac{1}{6}(\mathbf{F} \times \mathbf{F}) : \mathbf{F}$

Table 2: Kinematic set

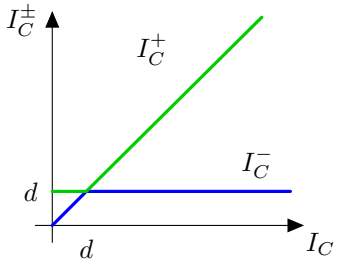

Fig. 1: Decomposition of the first invariant.

By making use of the deformation gradient $\mathbf{F}$, the area map $\mathbf{H}$ and the volume map J the strain energy function can be rewritten such that

$$\Psi(\mathbf{u}, \mathfrak{s}) = W(\mathbf{F}, \mathbf{H}, J, \mathfrak{s}). \tag{3}$$

Equation (3) eases the formulation of a polyconvex energy function which ensures the existence of a minimum, [6]. Further, the first Piola-Kirchhoff stress tensor is given by

$$\mathbf{P} = \frac{\partial W}{\partial \mathbf{F}} + \frac{\partial W}{\partial \mathbf{H}} \times \mathbf{F} + \frac{\partial W}{\partial J} \mathbf{H}. \tag{4}$$

For fracture only the tensile parts which are responsible for crack growth have to be considered. Hence, the strain energy function (3) is formulated by using the invariants $I_1 = \bar{\mathbf{F}} : \bar{\mathbf{F}}$ and $I_2 = \bar{\mathbf{H}} : \bar{\mathbf{H}}$ which are based on the isochoric split of the deformation gradient $\bar{\mathbf{F}} = J^{-1/3}\mathbf{F}$. The invariants are decomposed in compressive and tensile components $I_1^{\pm} = \langle I_1 - 3 \rangle^{\pm}$, $I_2^{\pm} = \langle I_2 - 3 \rangle^{\pm}$ and $J^{\pm} = \langle J - 1 \rangle^{\pm}$, cf. [6] and the split is demonstrated exemplarily for the first invariant in Fig. 1. The additive anisotropic split is formulated by

$$\tilde{I}_1(\bar{\mathbf{F}}, \mathfrak{s}) = g(\mathfrak{s}) I_1^+ + I_1^- + 3, \quad \tilde{I}_2(\bar{\mathbf{H}}, \mathfrak{s}) = g(\mathfrak{s}) I_2^+ + I_2^- + 3, \quad \tilde{J}(J, \mathfrak{s}) = g(\mathfrak{s}) J^+ + J^- + 1. \tag{5}$$

Inserting equations (5) into (3) the strain energy function can be rewritten $W(\mathbf{F}, \mathbf{H}, J, \mathfrak{s}) = W(\tilde{I}_1, \tilde{I}_2, J, \mathfrak{s})$. The total minimization problem is given in Table 1. The stresses $\boldsymbol{\sigma}$ of the linear material model coincide with the first Piola-Kirchhoff stress tensor $\mathbf{P}$ in (4).

2.3 Pressure induced fracture

Pneumatic fracture involves the injection of air or fluid at a sufficient pressure which induces crack propagation. In order to simulate pneumatic fracturing we consider a simplified approach of hydraulic fracture where the permeability is neglected and the pressure works as a boundary condition in a quasistatic setting. Here, the hydrostatic pressure p is seen as the driving force and is investigated by using the Terzaghi's principle of the stress tensor for both cases, the linear and non-linear material:

$$\boldsymbol{\sigma} = \boldsymbol{\sigma}^{\mathrm{eff}} - \bar{p} \cdot \mathbf{I}, \qquad \mathbf{P} = \mathbf{P}^{\mathrm{eff}} - \bar{p} \cdot \mathbf{H} \tag{6}$$

The hydrostatic pressure is modified by a linear increase coupled with the phase-field parameter assumed as $\bar{p} = p + \mathfrak{s} p_0$ with a given reference pressure p_0.

2.4 Discretization

Restated in the weak form, the coupled problem reads: Find $\mathbf{u} \in \mathcal{V}^u$ and $\mathfrak{s} \in \mathcal{V}^{\mathfrak{s}}$ such that

$$\int_\Omega \rho_0 \ddot{\mathbf{u}} \cdot \delta\mathbf{u} \, \mathrm{d}\Omega + \int_\Omega \boldsymbol{\sigma} : \nabla(\delta\mathbf{u}) \, \mathrm{d}\Omega = \int_\Omega \bar{\mathbf{b}} \cdot \delta\mathbf{u} \, \mathrm{d}\Omega + \int_{\partial\Omega} \bar{\mathbf{t}} \cdot \delta\mathbf{u} \, \mathrm{d}(\partial\Omega) \quad \forall \delta\mathbf{u} \in \mathcal{V}_0^u \,, \tag{7}$$

and

$$\int_\Omega \dot{\mathfrak{s}} \cdot \delta\mathfrak{s}\, \mathrm{d}\Omega + \int_\Omega \frac{\partial \Psi}{\partial \mathfrak{s}} \cdot \delta\mathfrak{s}\, \mathrm{d}\Omega + 2\mathcal{G}_c l_c \int_\Omega \nabla\mathfrak{s}\nabla(\delta\mathfrak{s})\, \mathrm{d}\Omega - \frac{\mathcal{G}_c}{2l_c}\int_\Omega (1-\mathfrak{s}) \cdot \delta\mathfrak{s}\, \mathrm{d}\Omega = 0 \quad \forall \delta\mathfrak{s} \in \mathcal{V}_0^{\mathfrak{s}}\,. \tag{8}$$

The functional space of admissible mechanical fields is $\mathcal{V}^u = \{\mathbf{u} \in \mathcal{H}^1(\Omega) \forall t \in [0,T]\}$, where $\mathcal{H}^1$ denotes the Sobolev functional space of square integrable functions with square integrable weak first derivatives. The notation $\mathcal{V}_0^u$ indicates the additional constraint $\delta\mathbf{u} = 0$ on $\partial\Omega$. In analogy the spaces of admissible phase-fields are $\mathcal{V}^{\mathfrak{s}} = \{\mathfrak{s} \in \mathcal{H}^1(\Omega) \forall t \in [0,T] | \mathfrak{s} \in [0,1]\}$ and $\mathcal{V}_0^{\mathfrak{s}} = \{\delta\mathfrak{s} \in \mathcal{V}^{\mathfrak{s}} | \delta\mathfrak{s} = 0 \text{ on } \partial\Omega(t)\}$. In equation (7) the stresses $\boldsymbol{\sigma}$ of the linear material model concur with $\mathbf{P}$ in (4).

2.5 Multigrid method of solution

In this section we focus on multigrid methods as solution technique, [5] which rely on a hierarchy V_l of usually nested finite element spaces. The subscript $l = 0, \ldots, L$ denotes the level and we assume $L \geq 1$ to be the finest level. In the case of geometric multigrid methods a hierarchy of nested meshes $(\mathcal{J}_l)_{0 \leq l \leq L}$ is constructed with a mesh-size h_l and a shape regular finite element triangulation $\mathcal{J}$ of the domain Ω. This mesh hierarchy is created by successively refining a given coarse mesh. Finally the solution process consists of two main components: the so called smoothing and the coarse grid correction. The smoothing reduces the respective high frequency errors on each level, in general using a simple iterative solver. Then the remaining low frequency error is removed by a direct solver on the coarsest level.

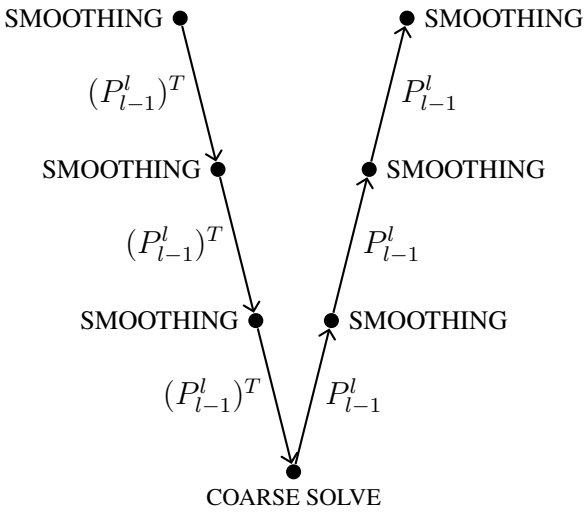

Fig. 2: Multigrid V-cycle.

In order to transfer between the subsequent spaces prolongation and restriction operators are used. This prolongation operator P_{l-1}^l maps coarse-grid correction to the next finer level and the restriction operator which is often chosen as $(P_{l-1}^l)^T$, transfers the fine level residual to the coarse level. The multigrid solver is based on a recursive structure. As a consequence information stemming from quadrature on the finest level L is used to assemble the coarse level operators. This fact is of major importance since the length-scale parameter l_c used in the phase-field model is tightly coupled to the mesh size h by means of the relation $h < \frac{l_c}{2}$. More details regarding this solution technique can be found in [2].

3 Numerical Examples

To demonstrate the accuracy and the performance of the proposed formulations two and three dimensional examples are considered. As a first example we simulate a three dimensional block of brittle rock material which is loaded in such a way, that it will crack by conchoidal fracture. This model has been suggested to work as a benchmark problem [7] in the framework of our DFG Priority Programme 1748 in order to test and validate the phase-field model. Hence, we investigate a $4a \times 4a \times 2a$ block of stone material and prescribe a displacement on part of its upper boundary of size $2a = 1$ m. The geometrical setup and the related boundary conditions of the problem are demonstrated in Fig. 3 in more detail. The mesh consists of $30 \times 30 \times 30$ eight-node brick elements.

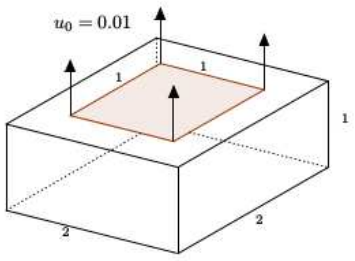

Fig. 3: Boundary conditions of the Benchmark problem.

The critical energy release rate is of $\mathcal{G}_c = 1\frac{\mathrm{N}}{\mathrm{mm}}$ and the material is chosen to be of Neo-Hookean type with parameters $\lambda = 100000\ \frac{\mathrm{N}}{\mathrm{mm}^2}$ and $\mu = 100000\ \frac{\mathrm{N}}{\mathrm{mm}^2}$ which is defined as

$$W(\mathbf{F}, J, \mathfrak{s}) = \frac{\mu}{2}(\tilde{I}_1 - d) + \frac{\kappa}{2}(\tilde{J} - 1)^2 \tag{9}$$

with the dimension $d \in \{2,3\}$, the shear modulus μ and the bulk modulus κ. The block cracks at a prescribed displacement of about 3 mm, see right plot in Fig. 4. Furthermore, in Fig. 4 the final state of the crack and the crack surface are displayed.

In the following the focus is set on pressure induced fracture. We consider a two dimensional plate of size 0.06 m $\times$ 0.06 m which consists of 256×256 Lagrangian-elements. As depicted in Fig. 5 the boundaries are clamped in all directions. Moreover, two cracks are initialized by setting the phase-field parameter $\mathfrak{s} = 1$. The pressure is then injected in these pre-cracks by modifying the stress tensor as proposed in (6). In this example the material is assumed to be of Neo-Hookean type with parameters $E = 210 \times 10^9\ \frac{\mathrm{N}}{\mathrm{m}^2}$ and $\nu = 0.3$, see Eq. (9). Moreover, the parameters for the phase-field description

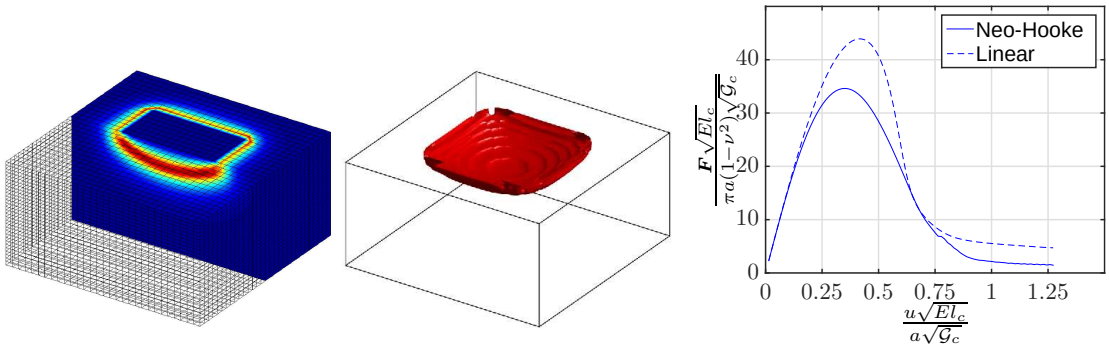

Fig. 4: Benchmark SPP1748, cf. [7], Final state, crack surface and force-displacement curve for the non-linear material model.

are chosen as $\mathcal{G}_c = 2.7 \times 10^3 \, \frac{\mathrm{J}}{\mathrm{m}^2}$ and $l_c = 4.6875 \times 10^{-4}$ m. The pressure is prescribed by a reference pressure given by $p_0 = 10^8 \, \frac{\mathrm{N}}{\mathrm{m}^2}$ which is increased incrementally during the simulation. A quasistatic calculation and a staggered scheme are applied. The snapshots of the phase-field are shown in Fig. 6.

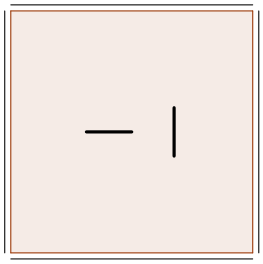

Fig. 5: Boundary conditions

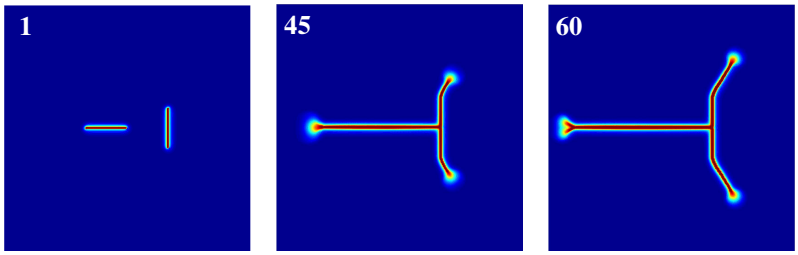

Fig. 6: Pressure driven process at different times $t \in \{1, 45, 60\}$ in two dimensions.

In three dimensions a bounded domain of size $0.5 \times 0.5 \times 0.5$ m is considered analogously whereby the boundaries are also clamped in all directions. The mesh consists of $50 \times 50 \times 50$ Lagrangian-elements. In compliance to the two dimensional example here five crack surfaces are prescribed by setting the phase-field parameter $s = 1$ and using the expressions (6). Here we set the focus on linear elasticity and make use of the related strain energy function (2). Moreover, the proposed multigrid method to solve the system of equations is applied. The material parameter are chosen as above. . The isosurfaces of the crack surfaces are demonstrated in Fig. 7 at different times. Further results of the different phase-field approaches and of pressure driven fracture can be found in [3].

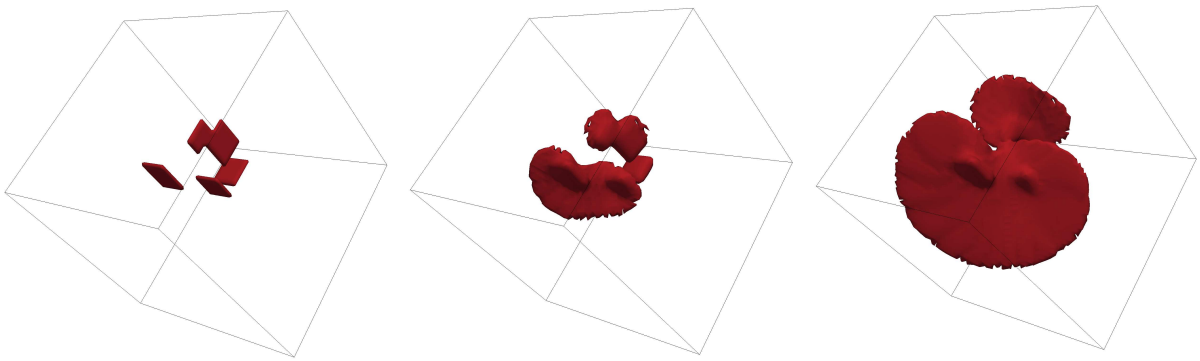

Fig. 7: Pressure driven process at different times $t \in \{1, 25, 100\}$ in three dimensions.

References

[1] L. Ambrosio and V. M. Tortorelli. via Γ-convergence. Communications on Pure and Applied Mathematics, **43(8)**:999–1036 (1990).
[2] C. Bilgen, A. Kopaničáková, R. Krause, and K. Weinberg. under review at Meccanica, (2017).
[3] C. Bilgen and K. Weinberg. submitted to Comput. Methods Appl. Mech. Engrg., (2017).
[4] J. Bonet, A. Gil, and R. Ortigosa. Comput. Methods Appl. Mech. Engrg., **283**:1061–1094 (2015).
[5] W. L. Briggs, S. F. McCormick, et al. Siam, (2000).
[6] C. Hesch, A. J. Gil, R. Ortigosa, M. Dittmann, C. Bilgen, P. Betsch, M. Franke, A. Janz, K. Weinberg. Comput. Methods Appl. Mech. Engrg., **317**: 649 - 683, (2017).
[7] R. Müller and C. Kuhn. Presentation at the Annual Meeting of SPP 1748 in Pavia, (2016).